Available online at www.sciencedirect.com
SCIENCE DIRECT®
Journal of Sound and Vibration 285 (2005) 149–171
JOURNAL OF SOUND AND VIBRATION
www.elsevier.com/locate/jsvi

Adaptive active control of flexural waves in a beam in the presence of a nearfield

C.R. Halkyard[a], B.R. Mace[b,*]

[a]*Department of Mechanical Engineering, University of Auckland, Private Bag 92019, Auckland, New Zealand*
[b]*Institute of Sound and Vibration Research, University of Southampton, Highfield, Southampton SO17 1BJ, UK*

Received 13 February 2003; received in revised form 11 August 2004; accepted 17 August 2004
Available online 7 December 2004

Abstract

This paper describes a wave-based, adaptive, feedforward system for the control of flexural waves in a beam when a significant nearfield wave is present. Many potential applications for active vibration control require a physically compact control system, in which the error sensors are located close to the control actuator. Because of the small physical size of the control system, there can be a significant nearfield wave as well as propagating waves in the vicinity of the error sensors, and the presence of this nearfield must be taken into account. An estimate of the downstream propagating wave amplitude is obtained by digitally filtering and combining the outputs of an array of three sensors, and is used as a cost function in a conventional filtered X-LMS adaptive algorithm. This has significant advantages over the more conventional approach in which the response at a single point is used as a cost function. Numerical simulations and experimental implementation of the control achieved with the wave-based and conventional systems are presented. It is seen that the wave-based system can offer significantly better broadband attenuation than the conventional approach in which response at a point is minimised.

1. Introduction

The use of an appropriate cost function in an adaptive control system can be critical to the system performance. Naturally, the choice of cost function depends strongly on the overall

*Corresponding author. Tel.: +44 23 8059 2344; fax: +44 23 8059 3190.
E-mail addresses: r.halkyard@auckland.ac.nz (C.R. Halkyard), brm@isvr.soton.ac.uk (B.R. Mace).

0022-460X/$ - see front matter © 2004 Elsevier Ltd. All rights reserved.
doi:10.1016/j.jsv.2004.08.024

Nomenclature

c	wave velocity
EI	flexural stiffness
e	error signal, base of natural log
$\mathbf{e}$	vector of injected wave amplitudes
f	frequency
$h(t)$	impulse response
$H(\omega)$	frequency response
k	wavenumber
l	distance between control actuator and centre of sensor array
n_d	number of delay terms in wave filter
r	reflection coefficient (complex scalar)
$\mathbf{r}$	reflection coefficient (complex matrix)
R	reflection coefficient (magnitude)
$v(t)$	velocity (time domain)
$V(\omega)$	velocity (frequency domain)
x	location coordinate
$\mathbf{W}$	vector of filter weights
$\mathbf{X}$	vector of filter inputs
α	constant relating wavenumber to frequency
Δ	sensor spacing
ε	$-\text{imag}(k)/\text{real}(k)$ (i.e. $k = \text{Re}\{k\}(1 - \text{i}\varepsilon)$)
ω	angular frequency
σ	beam mass per unit length
θ	phase
λ	wavelength
μ	adaptation parameter
τ	time delay
Φ	wave amplitude

Subscripts

C,c	control
e	error
g	group
k	kth time step
n	Nyquist frequency
N	nearfield
r	response
s	sampling rate or source
V	velocity
$+,-$	propagation/decay direction

objective of the control. If control of vibration at a point is desired, then the vibration level at that point is an obvious cost function, and this approach has been used in many studies (e.g. [1–4]). However, minimising vibration at a point does not guarantee low *overall* vibration levels in a structure. For better *global* performance it may therefore be preferable to use an alternative cost function, with one possibility being the amplitude of a propagating wave. In particular, one might choose to minimise the amplitude of the outward-propagating wave downstream of the control location, since it is this wave which propagates energy to the downstream region.

A wave propagation model has been used in active vibration control by a number of researchers (e.g. [5–9]). To use wave amplitude as a cost function, however, it is necessary to obtain real-time estimates of the required wave amplitude. A technique for obtaining estimates of flexural wave amplitude in a beam in real time, and the subsequent use of these estimates in active vibration control, has been described in earlier papers by the authors [10,11]. However, these papers only considered far-field conditions, allowing the effects of nearfields to be ignored. While this restriction was sufficient for demonstration of the concept, it resulted in a control system of limited applicability. The assumption of far-field conditions means that the error sensors should be placed a significant distance from any discontinuities, including the control actuator. The overall control system is consequently relatively large, and hence unsuitable for the many potential active vibration control applications. This paper addresses the aforementioned limitation by extending the approach described in [11] to include the effect of the nearfield

generated by the control actuator, and therefore allowing the use of a physically compact control system.

Specifically, this paper describes the application of wave-based adaptive control of vibrational energy flow to flexural vibration in beams, using a filtered-X LMS algorithm [12], where the error sensors are significantly influenced by the nearfield of the control actuator. It employs a systematic approach to wave amplitude estimation, that, while implemented using an array of equally spaced velocity sensors here, could equally well be implemented with other sensor types or combinations of sensor types, including distributed sensors. The wave decomposition approach described here avoids the use of finite-difference approximations that lead to systematic errors at high frequencies and ill-conditioning at low frequencies. The estimation of the wave amplitudes uses relatively short FIR filters, avoiding the stability-checking necessary with IIR filters while keeping computational requirements relatively low. The control strategy that is implemented minimises the square of the amplitude of a given propagating wave, and thus it controls a parameter that is proportional, in a frequency-weighted sense, to the vibrational energy flow in the specified direction. However, more elaborate control strategies could also be implemented based on knowledge of the wave amplitudes.

The following section describes the system being controlled, and this is followed by a description of the system behaviour in terms of waves. In Section 4, the real-time estimation of wave amplitudes is described. Further details can be found in [13]. Finally, the system is simulated numerically and implemented experimentally, and the results compared and discussed.

2. The system

In this paper, feedforward adaptive active control of flexural vibration in a beam is considered. A schematic diagram of the system is shown in Fig. 1. A disturbance is produced by some source, and excites vibrations of the beam by injecting waves at some point $x = x_s$. The waves travel through the structure producing unwanted vibrations in some remote region. A reference signal from the disturbance is assumed available, and this is input to the digital controller, which produces a control signal. This control signal is used to excite additional controlling vibrations by injecting further waves at $x = x_c$.

The resulting vibration field comprises waves, excited by both the disturbance and the control, which travel in both directions along the beam. In general, waves will be reflected from the ends of the beam. In one limiting case, where the amplitudes of these reflections are negligible, the beam appears to be infinitely long. In a finite beam, however, the reflections lead to resonant behaviour of the beam and the wave field becomes a superposition of travelling and standing waves. This can cause deterioration in the performance of the active control system.

The error sensor in Fig. 1 provides an error signal that gives some measure of the resulting vibrations. In this paper, an error sensor is defined in a general way: the error sensor is some array of one or more response sensors such as accelerometers, strain gauges, piezoelectric patches, etc.; these response sensors may measure point responses or may be distributed; the outputs of the response sensors may also be combined and filtered, using either analogue or digital filters or both, and the resulting output signal is defined as being the error signal. The error signal is used to perform two functions. The first is to quantify the control achieved, while the second is to provide

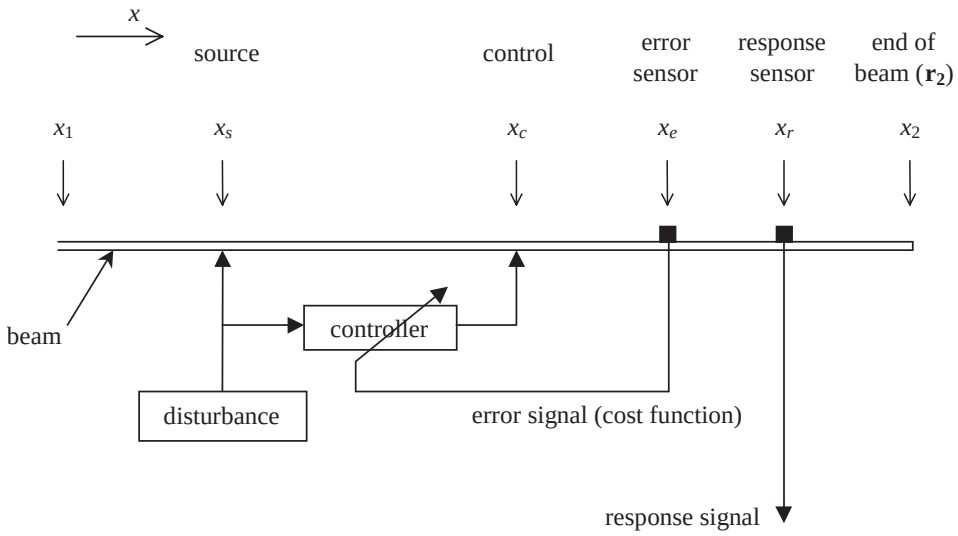

Fig. 1. Feedforward control of bending vibrations.

a cost function that may be used to adaptively change the controller parameters to improve performance. In the simulations and experiments described, a filtered-X LMS algorithm is used for adaptation, but other adaptive algorithms may also be used. Three different error sensor types will be considered. The first is a conventional sensor that measures the response at a point. The second is an array of two sensors, the outputs of which are digitally filtered and combined to provide an estimate of the positive-going propagating wave amplitude under the assumption of far-field conditions. This type of sensor array is described in more detail in [11]. The third type of error sensor uses an array of three sensors to provide an estimate of the positive-going propagating wave amplitude. The processing of the three sensor outputs allows for the presence of a positive-going nearfield, and thus permits the sensor array to be placed close to the control actuator. This approach is the subject of the paper, with the other two error sensor types being used for comparative purposes.

3. Structural dynamic variables and error sensors

3.1. The system and waves

Consider, for the time being, time harmonic behaviour at frequency $\omega\cdot$ The behaviour of the beam may be written in terms of propagating and nearfield wave amplitudes. These waves may be defined in terms of any dynamic variable, such as displacement or strain, but in this paper they will be defined in terms of transverse velocity. In the vicinity of the error sensor, which is immediately downstream of the control actuator, the transverse velocity of the beam is assumed

to be given in terms of these velocity wave components by

$$V(x,\omega) = \Phi_V^+(\omega)\mathrm{e}^{-\mathrm{i}kx} + \Phi_{N,V}^+(\omega)\mathrm{e}^{-kx} + \Phi_V^-(\omega)\mathrm{e}^{\mathrm{i}kx}, \tag{1}$$

where Φ_V^+ and Φ_V^- are the amplitudes of the propagating waves and $\Phi_{N,V}^+$ is the residual nearfield produced by the control. It is assumed that the amplitude of the upstream-going nearfield $\Phi_{N,V}^-\exp(kx)$ is negligible: this wave would typically be produced by reflections from the end at $x = x_2$ (or some other discontinuity), and would decay exponentially with distance from that end. At a distance of a half-wavelength from the end this nearfield will have attenuated to about 4% of its original amplitude, and the assumption that its contribution to the motion in this region is negligible will generally be justified. Strictly, the assumption requires $\exp(-k|x_e - x_2|) \ll 1$. In Eq. (1) k is the wavenumber, where

$$k = \alpha\sqrt{\omega}; \quad \alpha = \sqrt[4]{\sigma/EI}, \tag{2}$$

EI being the flexural stiffness of the beam and σ is its mass per unit length (a list of symbols is given in the appendix). In the presence of damping k has a (usually small) negative imaginary part so that the amplitude of a propagating wave component decays gradually in the direction of propagation. The damping can therefore be characterised by

$$\varepsilon = -\frac{\mathrm{Im}(k)}{\mathrm{Re}(k)} \;\Rightarrow\; k = \mathrm{Re}(k)(1 - \mathrm{i}\varepsilon). \tag{3}$$

In this paper, it will be assumed that the decay of the propagating wave amplitude is negligible over distances of the order of the length of the sensor array. The nearfield of the disturbance is assumed to be negligible, while that of the control is included since the control may be applied close to the error sensor array and this may adversely affect the performance of the system. The downstream propagating wave,

$$\Phi_V^+ = \Phi_{V,D}^+ + \Phi_{V,C}^+ \tag{4}$$

is the superposition of components from the disturbance and control. These may be considered as arising from the reference signal being filtered by the primary and secondary paths, respectively.

The upstream propagating wave,

$$\Phi_V^- = \Phi_{V,0}^- + r\Phi_V^+; \quad r = R\,\mathrm{e}^{-\mathrm{i}\theta_r} \tag{5}$$

also has two components. The first, $\Phi_{V,0}^-$, is produced by any additional vibration sources that may happen to act downstream of the error sensor array (i.e. at $x > x_e$), Φ_V^+ and $\Phi_{V,0}^-$ being incoherent. (Henceforth it will be assumed that this component is negligible unless otherwise stated.) The second component, $r\Phi_V^+$, arises from the coherent reflection of Φ_V^+ from downstream boundaries or attachments. The reflection coefficient r is complex, its magnitude R being less than or equal to 1 and its phase $(-\theta_r)$ is typically negative and decreases monotonically. It cannot be assumed that the magnitude of this reflected wave is negligible.

The performance of the control system will depend on the nature of the wave field that is present, and on the cost function used. Two possible cost functions are considered in the following subsection: velocity and downstream-going propagating wave amplitude.

3.2. Structural dynamic variables as cost functions

3.2.1. Velocity as a cost function

Consider the case of a single velocity sensor mounted at $x = x_e$, and for simplicity use a coordinate system such that $x_e = 0$. If the output of this sensor is used as a cost function, then an ideal controller will force the velocity at that point to be zero. From Eq. (1) it follows that

$$\Phi_V^+ + \Phi_{N,V}^+ + \Phi_V^- = 0. \tag{6}$$

Since $\Phi_V^- = r\Phi_V^+$,

$$\Phi_V^+ = -\frac{1}{1+r}\Phi_{N,V}^+ \tag{7}$$

and hence the required control effort is

$$\Phi_{V,C}^+ = -\frac{1}{1+r}\Phi_{N,V}^+ - \Phi_{V,D}^+. \tag{8}$$

A distance x further downstream the velocity will be

$$V(x,\omega) = -\frac{1}{1+r}\Phi_{N,V}^+(\omega)(\mathrm{e}^{-\mathrm{i}kx} + r\mathrm{e}^{\mathrm{i}kx}) + \Phi_{N,V}^+(\omega)\mathrm{e}^{-kx}. \tag{9}$$

Three points should be noted. First, the nearfield deteriorates the performance, giving rise to some residual response away from the error sensor location. If a compact control system is required (i.e. if the spacing between the error sensor and control actuator is small) then this could be substantial. Secondly, global control is not achieved, although the residual downstream vibrations would be small if the nearfield at the error sensor location $\Phi_{N,V}^+$ and R are small. Finally, reflections can cause substantial problems at certain frequencies, especially if $R \approx 1$, since $1/(1+r)$ can become very large if θ_r is an odd multiple of π. This is particularly true for lightly damped, finite structures, which are often the target for control. In effect, at these frequencies the sensor is mounted at or close to a node of a standing wave originating at the boundary. The frequencies can be dense, since $\theta_r \sim 2kl_b$, where l_b is the distance to the boundary, which may be large. The frequencies are also typically difficult to predict accurately, since they are sensitive to changes or uncertainties in the system properties such as the wavenumber or the boundary conditions (e.g. changes in orientation, payload etc.). It would therefore be difficult to compensate for the term $1/(1+r)$ in a robust manner.

3.2.2. Wave amplitude as a cost function

If the positive-going wave amplitude Φ_V^+ is sensed at $x = x_e = 0$ and used as a cost function, the control adapts so that Φ_V^+ is zero. The residual velocity for $x \geqslant x_e$ is then

$$V(x,\omega) = \Phi_{N,V}^+(\omega)\mathrm{e}^{-kx} \tag{10}$$

and comprises solely the nearfield of the control. Thus there is some localised response, but global control is achieved and the effects of downstream reflections are irrelevant. The required control effort is, from Eq. (4),

$$\Phi_{V,C}^+ = -\Phi_{V,D}^+ \tag{11}$$

so that the control merely involves cancellation of the propagating wave. It is therefore apparent that there may be significant benefits in using wave amplitude as a cost function. However, conventional sensors measure the effects of the superposition of all wave components. In order to estimate the amplitude of an individual wave component it is necessary to filter and combine the outputs of a number of sensors. A method by which the amplitude of a given wave can be estimated in the absence of nearfields, and used as a cost function in adaptive vibration control, is described in [11]. In this paper, the presence of the nearfield from the control actuator is included.

The error sensor array must lie an appropriate distance from the control actuator if the amplitude of the nearfield from the control is to be negligible. If this is not possible due to space constraints, the contribution of the nearfield to the measured motion will not be negligible, and will introduce an additional error to the amplitude estimate, with a consequent adverse effect on the attenuation achieved. Therefore, to implement a compact and effective control system of this type, it is necessary to obtain a reliable estimate of propagating wave amplitude in the presence of a nearfield. A method of obtaining such an estimate is described in the following section.

4. Wave amplitude estimation

The estimates of wave amplitude are obtained by digitally filtering and combining the outputs of an array of three sensors, the placement of which is shown in Fig. 2. In this section, the design of appropriate filters is described. The characteristics of the ideal filters are determined in the frequency domain, and these are then approximated with FIR filters. Details of the approach and the design and performance of the filters are given in [13].

4.1. Frequency domain decomposition

Suppose that the sensors measure transverse velocity. If the nearfield $\Phi^-_{N,V}$ is ignored, then the velocity in the region around the array can be written in terms of transverse velocity waves as

$$V(x,\omega) = \Phi^+_V e^{-ikx} + \Phi^+_{N,V} e^{-kx} + \Phi^-_V e^{ikx}. \tag{12}$$

Taking $x_e = 0$ for convenience, the vector of sensor outputs can therefore be expressed as

$$\mathbf{Y}(\omega) = \begin{Bmatrix} V_1(\omega) \\ V_2(\omega) \\ V_3(\omega) \end{Bmatrix} = \begin{Bmatrix} V(-a,\omega) \\ V(0,\omega) \\ V(a,\omega) \end{Bmatrix} = \mathbf{S}(\omega)\mathbf{\Phi}(\omega), \tag{13}$$

where

$$\mathbf{S}(\omega) = \begin{bmatrix} e^{ika} & e^{-ika} & e^{ka} \\ 1 & 1 & 1 \\ e^{-ika} & e^{ika} & e^{-ka} \end{bmatrix}; \quad \mathbf{\Phi}(\omega) = \begin{Bmatrix} \Phi^+_V(\omega) \\ \Phi^-_V(\omega) \\ \Phi^+_{N,V}(\omega) \end{Bmatrix}, \tag{14}$$

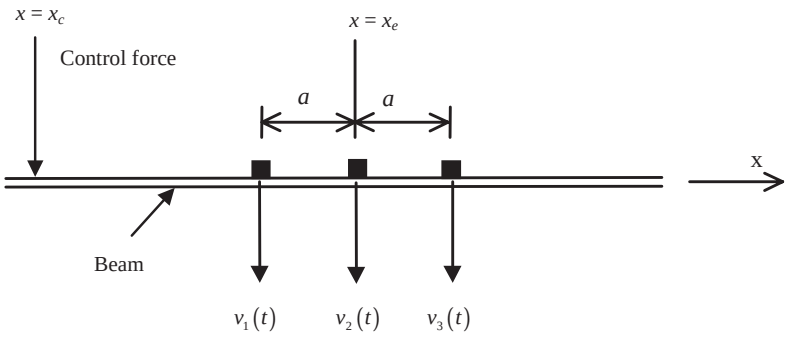

Fig. 2. Error sensor array comprising three velocity sensors.

and where $\mathbf{\Phi}$ is the vector of wave amplitudes at the centre of the array. These wave amplitudes are consequently given by

$$\mathbf{\Phi}(\omega) = \mathbf{G}(\omega)\mathbf{Y}(\omega), \tag{15}$$

where

$$\mathbf{G}(\omega) = \mathbf{S}^{-1}(\omega). \tag{16}$$

The frequency response matrix $\mathbf{G}(\omega)$ can therefore be found by inverting $\mathbf{S}(\omega)$. The determinant of $\mathbf{S}$ equals $4\mathrm{i}\sin ka(\cosh ka - \cos ka)$, and hence $\mathbf{S}$ is singular if the separation, a, is half a wavelength: this imposes an upper frequency limit for any given array.

As defined above, the matrix $\mathbf{G}$ provides wave amplitudes of the same response variable as the sensor outputs, i.e. displacement measurements give displacement wave amplitudes. Similarly, acceleration measurements would give acceleration wave amplitudes. This need not be the case, however. For example, if the sensors measure velocity, then $\mathbf{G}$ would provide estimates of velocity-wave amplitudes, while $\mathrm{i}\omega\mathbf{G}$ and $\mathbf{G}/(\mathrm{i}\omega)$ would provide estimates of acceleration-wave and displacement-wave amplitudes, respectively.

4.2. Time domain reconstruction

In general, more than one frequency component will be present and any wave amplitude is given by superposition of these frequency components. Thus,

$$\phi(t) = F^{-1}\{\mathbf{\Phi}(\omega)\} = F^{-1}\{\mathbf{G}(\omega)\mathbf{Y}(\omega)\} = \int_{-\infty}^{\infty} \mathbf{\Phi}(\omega)\mathrm{e}^{\mathrm{i}\omega t}\,\mathrm{d}\omega, \tag{17}$$

where $F^{-1}\{\cdot\}$ is the inverse Fourier transform. Since the inverse transform of a product is equal to the convolution of the individual inverse transforms, then

$$\phi(t) = \mathbf{g}(t) * \mathbf{y}(t), \tag{18}$$

where $*$ denotes convolution and $\mathbf{g}(t)$ is a matrix of impulse responses, which are the inverse Fourier transforms of the elements of $\mathbf{G}(\omega)$. In a practical implementation, approximations to these ideals are found. This paper considers only digital implementation, with FIR filters being used. The steps in implementing the wave filters are thus to specify the details of the sensor array,

to determine the matrices $\mathbf{S}(\omega)$ and $\mathbf{G}(\omega)$, and to design filters whose impulse responses approximate $\mathbf{g}(t)$ to acceptable accuracy. Details are given in [13].

A particular issue in the design of the filters is that of causality. The ideal impulse responses are non-causal, and these must be represented with a causal approximation. Previous work has shown that the introduction of a time delay in the filters improves the accuracy achievable with a given length of filter [10,11]. In the time-delay approach, an $n_t = (2n_d + 1)$ term filter is designed by time-delaying the filters by n_d time steps. This involves multiplying the ideal frequency response by $\exp(-\mathrm{i}\omega n_d)$. The output of the error sensor at each time step is thus an estimate of the wave amplitude n_d time steps before. Under these circumstances there must clearly be a compromise between accuracy and time delay. Increasing the filter length increases the frequency range over which the filter approximates the desired frequency response with acceptable accuracy. However, this also increases the inherent time delay, which can have an adverse effect on the control achieved.

5. Simulations

5.1. Physical system

The system being considered is shown in Fig. 1, with $x_1 \leqslant x_s \leqslant x_c < x_e \leqslant x_r \leqslant x_2$. It is assumed that there are no reflections at end 1 (i.e. the end for which $x < x_s$) while reflections can occur from the end 2 at $x = x_2$. Of interest is the total vibrational level in the region $x > x_c$, and the response is found at one or more points $x = x_r$, where x_r lies in some region between x_c and x_2. The effectiveness of the control is assessed in terms of the rms velocity at the response point before and after control. It should be noted that while the effect of the negative-going nearfield was ignored in the design of the wave filters, it has been included in the simulation of beam response. The performance of the control system can therefore be simulated when the assumption of a negligible negative-going nearfield is violated.

5.2. System dynamics

5.2.1. Sensor and actuator dynamics

The disturbance and control actuators apply forces to the beam. It is assumed that the actuators have perfect dynamics, in that the force produced per unit input signal is a constant, independent of frequency. Similarly, the velocity sensors are assumed to have frequency-independent dynamics, with constant unity gains.

5.2.2. Beam response

In the simulations the end at $x = x_2$ is taken to have a matrix of reflection coefficients $\mathbf{r_2}$. This matrix relates the amplitudes of the reflected propagating and nearfield waves $[\Phi^-(\omega) \quad \Phi_N^-(\omega)]^{\mathrm{T}}$ to those of the incident waves $[\Phi^+(\omega) \quad \Phi_N^+(\omega)]^{\mathrm{T}}$. It may take many values, for example,

$$\mathbf{r}_{2,a} = \begin{bmatrix} 0 & 0 \\ 0 & 0 \end{bmatrix}; \quad \mathbf{r}_{2,ss} = \begin{bmatrix} -1 & 0 \\ 0 & -1 \end{bmatrix}; \quad \mathbf{r}_{2,f} = \begin{bmatrix} -\mathrm{i} & 1+\mathrm{i} \\ 1-\mathrm{i} & -\mathrm{i} \end{bmatrix} \tag{19}$$

for an anechoic termination, for a simply supported end or for a free end respectively. Note that these reflection coefficients are independent of the variable used to define the wave amplitude, and hence the subscript V (denoting velocity) has been dropped from the incident and reflected wave amplitudes.

The frequency response of a thin beam is such that a time harmonic force $F\exp(\mathrm{i}\omega t)$ injects velocity waves of amplitudes [2]

$$\Phi_V^+(\omega) = \Phi_V^-(\omega) = \frac{k}{\omega}\frac{F}{4\sigma},$$
$$\Phi_{N,V}^+(\omega) = \Phi_{N,V}^-(\omega) = -\mathrm{i}\frac{k}{\omega}\frac{F}{4\sigma}, \tag{20}$$

where Φ_V^+ and Φ_V^- are the amplitudes of the positive- and negative-going propagating waves at the excitation point, and $\Phi_{N,V}^+$ and $\Phi_{N,V}^-$ are those of the nearfields.

Suppose that a force is applied at some point. Waves leave the excitation point with amplitudes defined by Eq. (20). After they propagate over a distance x the amplitudes become

$$\mathbf{H}_x(x;\omega) = \mathbf{fe}; \quad \mathbf{f} = \begin{bmatrix} \mathrm{e}^{-\mathrm{i}kx} & 0 \\ 0 & \mathrm{e}^{-kx} \end{bmatrix}; \quad \mathbf{e} = \frac{\beta}{\sqrt{\omega}}\begin{Bmatrix} 1 \\ -\mathrm{i} \end{Bmatrix}; \tag{21}$$

where $\mathbf{f}(x)$ is a propagation matrix, $\mathbf{e}$ the vector of injected wave amplitudes (Eq. (20)) and $\beta = \alpha F/4\sigma$ is a constant that depends on the excitation level and the beam properties. For convenience, it is assumed that $\beta = 1$. The velocity at x is given in terms of the velocity wave amplitudes by

$$V(x,\omega) = \begin{bmatrix} 1 & 1 \end{bmatrix}\mathbf{H}_x(x,\omega). \tag{22}$$

In the real-time simulations, impulse responses, rather than frequency response functions, are required. In principle, this merely involves finding the inverse Fourier transform of $\mathbf{H}_x$. However, difficulties arise in practice for the following reasons. First, $\mathbf{H}_x$ becomes infinite at $\omega = 0$ (i.e. a constant force produces constant acceleration and hence infinite velocity in the "steady state"). Secondly, in a digital implementation problems arise for frequency components above the Nyquist frequency. If these higher frequencies are not removed then their aliases contribute to $\mathbf{H}_x$. However, if they are ignored by simply neglecting them, the resulting impulse responses are non-causal. Finally, if they are removed by filtering then, in effect, $\mathbf{H}_x$ must be passed through a low-pass filter, so that the effective frequency response differs from $\mathbf{H}_x$ of Eq. (21). In the simulations, $\mathbf{H}_x$ is band-pass filtered in the range $(0.05f_n$–$0.95f_n)$ to remove the low and high frequency components.

5.2.3. *Propagation paths*

The response of the beam is described in terms of propagation paths between the two sources of excitation (disturbance and control), and the various points at which knowledge of the response is required. The *primary paths* are the paths between the disturbance source input and the individual sensors in the error sensor array. The *cancellation paths* are the paths between the control force input and the individual error sensors, and the *response paths* are the paths between the disturbance source and the control force inputs and the response sensor.

The frequency responses of each of these paths have two components, namely a *direct component* and a *reflected component*, which is merely the reflection of the direct component from the end at $x = x_2$. For example, the frequency response relating the response sensor output to the control force input is given by

$$H_{c,r}(\omega) = \begin{bmatrix} 1 & 1 \end{bmatrix} \mathbf{f}(x_r - x_c; \omega)\, \mathbf{e} + \begin{bmatrix} 1 & 1 \end{bmatrix} \mathbf{f}(x_2 - x_r; \omega)\, \mathbf{r}_2\, \mathbf{f}(x_2 - x_c; \omega)\, \mathbf{e}, \tag{23}$$

where the first term gives the direct component and the second term the component reflected from the end $x = x_2$.

In this paper, these are implemented using FIR filters, the frequency responses of which approximate those of the required paths with acceptable accuracy. The accuracy of the simulations is thus dependent on these filters being of sufficient length.

5.3. Control system

Digital control is implemented, using FIR filters for all filtering operations. The control filter is adaptive, using a filtered-X LMS algorithm. In this the updated filter weights are calculated from the expression

$$\mathbf{W}_{k+1} = \mathbf{W}_k + 2\mu e_k \mathbf{X}_k, \tag{24}$$

where $\mathbf{W}_k$ is the vector of filter weights, e_k is the error sensor output and $\mathbf{X}_k$ is the vector of inputs, with the subscript denoting the kth time step [12]. The constant μ is an adaptation parameter that determines the speed and stability of adaptation, with too small a value resulting in slow adaptation, and too large a value resulting in poor attenuation or instability. The parameters used in the simulations are given in Table 1. Controller parameters have been chosen to give moderately low-order models that demonstrate the physical behaviour that is typically observed.

5.4. Numerical examples

Real-time simulations of adaptive control were performed using Matlab® and Simulink®. Anechoic and free terminations were simulated, to illustrate the effects of reflections from the end. Three different cost functions were used. These were:

1. An estimate of positive-going propagating wave amplitude obtained from the three velocity sensors under the assumption of a significant positive-going nearfield, as outlined in the previous section.
2. An estimate of positive-going propagating wave amplitude obtained from a pair of velocity sensors under the assumption of far-field conditions, as described in [11]. Unless otherwise stated, these sensors are the right-hand pair (i.e. those most distant from the control actuator) of the three-sensor array.
3. Velocity at a point. Unless otherwise stated, this is obtained from the right-hand error sensor (i.e. the error sensor most distant from the control actuator) of the three-sensor array.

Simulations were run for 100 s, with the average responses over a 20 s period from $t = 80$ s being found. In simulations of the anechoic termination, the response point was arbitrarily chosen at

Table 1
Parameters used in simulation

Sample rate f_s	2048 Hz
Nyquist frequency $f_n = f_s/2$	1024 Hz
Wavelength at Nyquist frequency	λ_n
Damping ε	0.001
Frequency range	$0.05f_n$–$0.95f_n$
Wave filter length n_t	11 terms ($n_d = 5$)
Cancellation path filter length	32 terms
Control filter length	64 terms
Adaptation parameter μ	0.0001
Sensor spacing Δ	$0.1\,\lambda_n$
x_s (far-field simulation)	0
(single nearfield simulation)	$1.94\,\lambda_n$
(double nearfield simulation)	$3.65\,\lambda_n$
x_c (far-field simulation)	$2.15\,\lambda_n$
(single nearfield simulation)	$4.09\,\lambda_n$
(double nearfield simulation)	$5.90\,\lambda_n$
x_e (far-field simulation)	$4.30\,\lambda_n$
(single nearfield simulation)	$4.30\,\lambda_n$
(double nearfield simulation)	$6.00\,\lambda_n$ (centre of 3 sensor array)
	$6.175\,\lambda_n$ (centre of 2 sensor array)
x_r	$6.45\,\lambda_n$
x_2	$6.45\,\lambda_n$

some distant downstream location, while for the free end simulations the end of the beam was used as the response point. Three different scenarios are considered:

1. The error sensor array is distant from both the control actuator and the end of the beam, and thus nearfields are negligible. This is referred to as the "far-field" simulation.
2. The error sensor array is close to the control actuator, but sufficiently distant from the end of the beam for the negative-going nearfield to be negligible. This is referred to as the "single nearfield" simulation.
3. The error sensor array is close to both the control actuator and the beam end. This is referred to as the "double nearfield" simulation.

The results of the simulations are shown in Figs. 3–6. These figures show the rms response after control compared to that before control. Stated attenuations refer to the total attenuation attained over the frequency band $0.1f_n$–$0.9f_n$.

The performances of the three control systems in the "far-field" simulations, when the error sensors are located outside the nearfield of the control actuator, are shown for anechoic and free end conditions in Figs. 3 and 4, respectively. (Precise locations of the various components of the control system for all simulations are given in Table 1.) It can be seen in Fig. 3 that all three systems give very similar performance under anechoic conditions, with an overall attenuation of approximately 26.5 dB. The similarity in performance is to be expected because, in this case, all

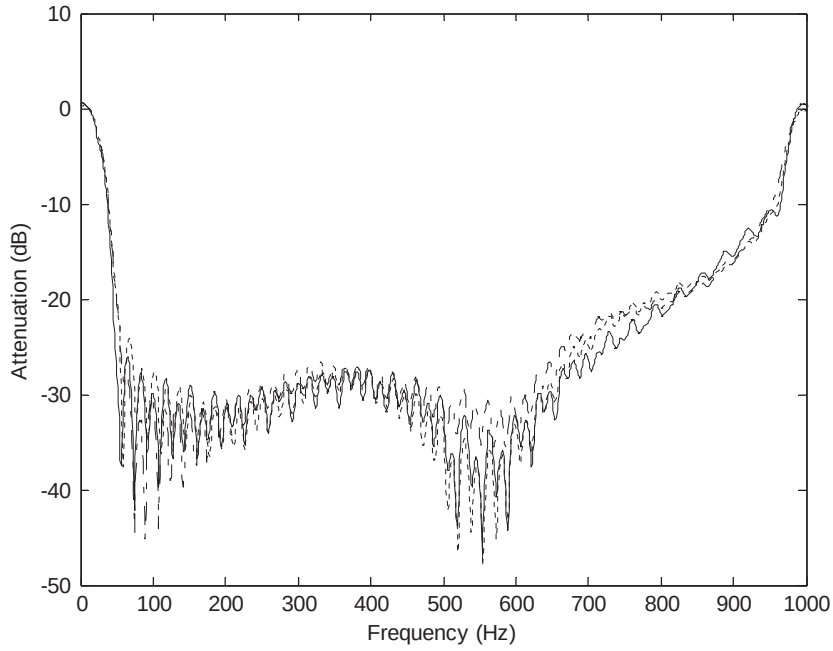

Fig. 3. Simulated attenuation (anechoic conditions, error sensor in far field) using different cost functions: ——— point velocity; – – – – propagating wave amplitude (far-field array); – - – - – propagating wave amplitude (nearfield array).

three cost functions are good indicators of the overall 'downstream' behaviour of the beam. Discrepancies arise due to the implemented filters being approximations of the ideal. It can be expected that the wave-based control systems will give a slightly poorer performance in this idealised case, as they utilise a greater number of filtering operations, and these provide no benefit when the error sensor is subjected only to a downstream-propagating wave. In practice, however, this effect may be reduced or negated through the 'averaging' effect of the additional sensors reducing sensitivity to measurement noise.

In Fig. 4 are shown the performances of the three control systems in the presence of an additional, reflected, upstream-propagating wave. This is caused by the beam having a free end, rather than an anechoic termination. In other ways, this simulation is identical to the previous case. It is apparent that the performances of the two wave-based systems are not significantly affected by the presence of the upstream-propagating wave, with the overall attenuation still being better than 26 dB. In contrast, the velocity-based control system exhibits distinct frequency bands in which attenuation is poor, and the overall attenuation is approximately 23 dB. These bands of poor attenuation correspond to frequencies at which the error sensor is at, or close to, a node of the standing wave that exists downstream of the control actuator [14].

The performances of the three control systems in the presence of a single nearfield are shown in Fig. 5. In this case, the error sensors are sufficiently close to the control actuator for the resulting nearfield to be significant, but are sufficiently distant from the free end of the beam for the negative-going nearfield to be ignored. It is apparent that the three-sensor (wave-based, near field)

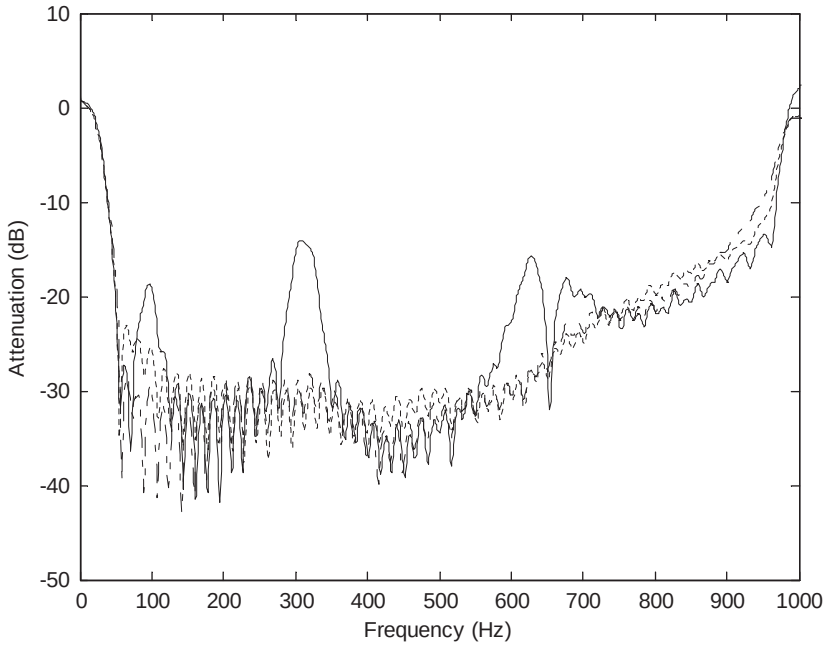

Fig. 4. Simulated attenuation (free end, error sensor in far field) using different cost functions: ———point velocity; – – – – propagating wave amplitude (far-field array); – - – - – propagating wave amplitude (nearfield array).

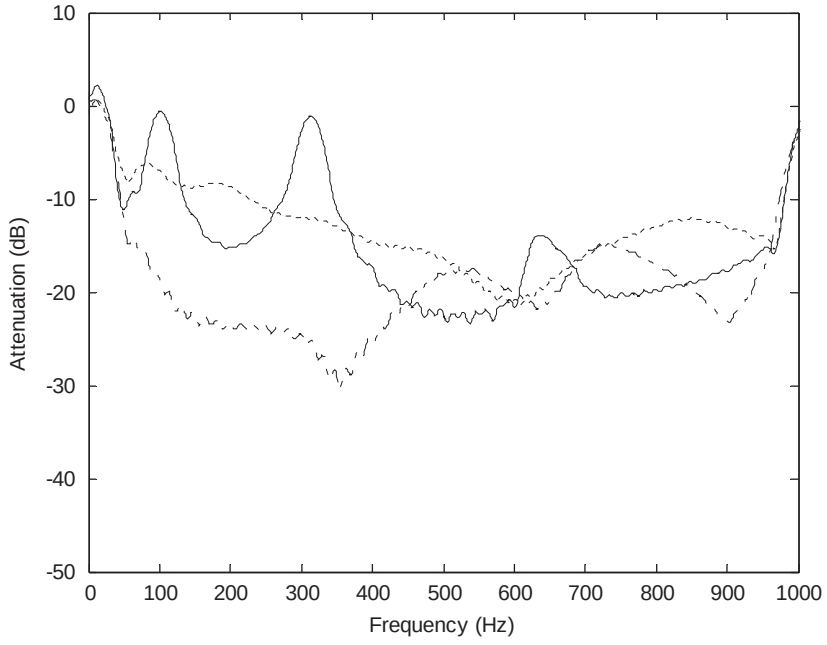

Fig. 5. Simulated attenuation (free end, error sensor in single nearfield) using different cost functions: ———point velocity; – – – – propagating wave amplitude (far-field array); – - – - – propagating wave amplitude (nearfield array).

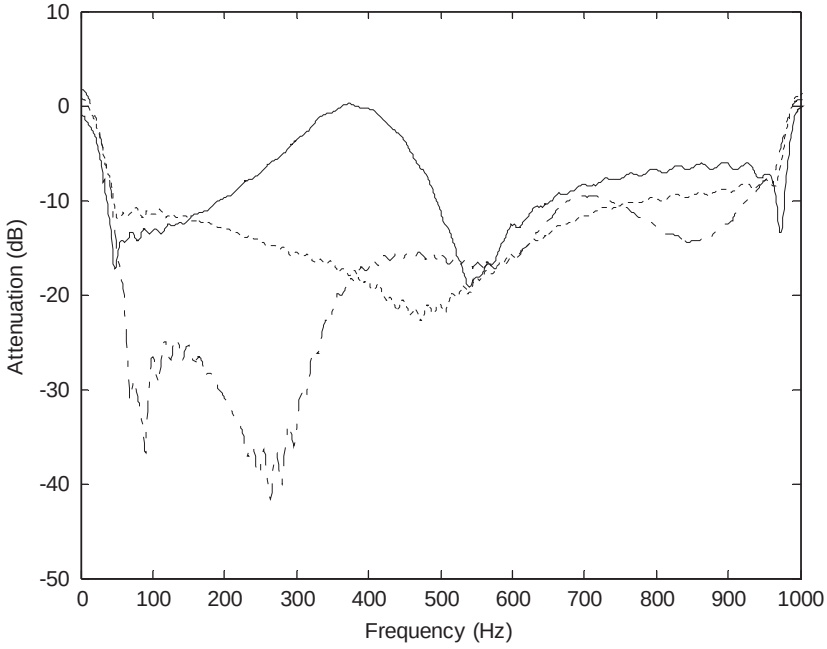

Fig. 6. Simulated attenuation (free end, error sensor in double nearfield) using different cost functions: ——— point velocity; – – – – propagating wave amplitude (far-field array); – - – - – propagating wave amplitude (nearfield array).

system gives substantially better performance than either of the other two systems at low frequencies. At higher frequencies the difference in performance between the two wave-based systems is less significant, because the effects of the nearfield become smaller. This is because the wavenumber $k = \alpha\sqrt{\omega}$ increases with frequency, while the nearfield decays as exp $(-kx)$ and thus becomes more localised as frequency increases. The two-sensor (wave-based, far-field) system thus gives an acceptable estimate of the downstream propagating wave amplitude under these circumstances. The single sensor (point velocity) system again exhibits regions of good performance separated by frequency ranges in which attenuation is poor. Overall attenuations are around 9, 11 and 21 dB for the point velocity, far-field wave and nearfield wave-based systems, respectively.

The effects of space limitations on the three control systems are shown in Fig. 6, which shows the results of the ''double nearfield'' simulation. In this case it is assumed that the control actuator is placed close to the end of the beam, so that both the positive-going and negative-going nearfields (i.e. those generated by the control actuator and the free end, respectively) are significant throughout the region between the actuator and the end of the beam. For the purposes of this simulation, the sensors for the velocity-based and far-field wave-based control systems are centred mid-way between the control actuator and the end of the beam, in the region where the nearfields are smallest. The sensors for the nearfield wave-based control system are placed close to the control actuator, in the region where the negative-going nearfield is smallest. It can be seen that the three-sensor system provides substantially better attenuation than the other two systems,

particularly at low frequencies. Overall attenuations are around 6, 13 and 17 dB for the point velocity (single sensor), far-field wave-based (two sensor) and nearfield wave-based (three sensor) systems, respectively. This is because the three-sensor system can be placed in a region where the conditions approximate those assumed in its design (i.e. motion dominated by two propagating waves and a positive-going nearfield). At low frequencies, the influence of one or more nearfields is significant at all points within the region. This violates the assumption of far-field conditions that is inherent in the velocity-based and far-field wave-based systems, and results in the poor performance of these systems. At higher frequencies the nearfields become less significant in the vicinity of the error sensors, and the performance of these 'far-field' systems starts to improve. However, the system using the single velocity sensor will exhibit poor attenuation at frequencies that result in the sensor being close to a node, as noted earlier.

6. Experimental measurements

6.1. Experimental set-up

The experimental set-up comprised a steel beam having dimensions 6000 mm × 50 mm × 6 mm suspended using piano wire at four points along its length. The 'upstream' end of the beam was embedded in a sandbox to approximate an anechoic termination, while the 'downstream' end of the beam was left free, giving strong reflection of any incident propagating wave.

Excitation was supplied using a Ling V201 electrodynamic shaker, driving the centre of the beam through a stinger rod, while the control force was applied through an identical system located 1 m 'downstream' of the disturbance actuator, as shown in Fig. 7. The error sensor array comprised three PCB 353B65 piezo-electric accelerometers separated by a distance of $23.5\,\text{mm} \approx 0.1\,\lambda_n$, where λ_n is the wavelength at the Nyquist frequency, and centred on a point 47 mm from the control actuator. This resulted in a compact control system, but placed the error sensors so that the nearfield of the control actuator was of some significance. Three PCB 353B65 accelerometers were placed downstream of the error sensor array, as shown in Fig. 7, to monitor the control system performance. The output of the sensor at the beam tip has been used in the presentation of the experimental results. In all cases the sensor outputs were integrated to give signals proportional to velocity.

The disturbance and control signals were generated by a Pentium II® 350 MHz PC (incorporating 64 Mb of RAM), equipped with a Keithley Metrabyte® 1600 Series A-D/D-A board. All real-time processing was performed using Matlab® and Simulink® software, incorporating the Real-Time Workshop® and the Real-Time Windows Target®. The disturbance signal, the control signal and the response were also monitored using a Hewlett Packard HP® 3566A 8-channel analyser. Parameters used in the experimental measurements are given in Table 2.

6.2. Experimental procedure

Two control systems were implemented on the beam. The first of these utilised three sensors to provide an estimate of the positive-going propagating wave amplitude in the presence of a

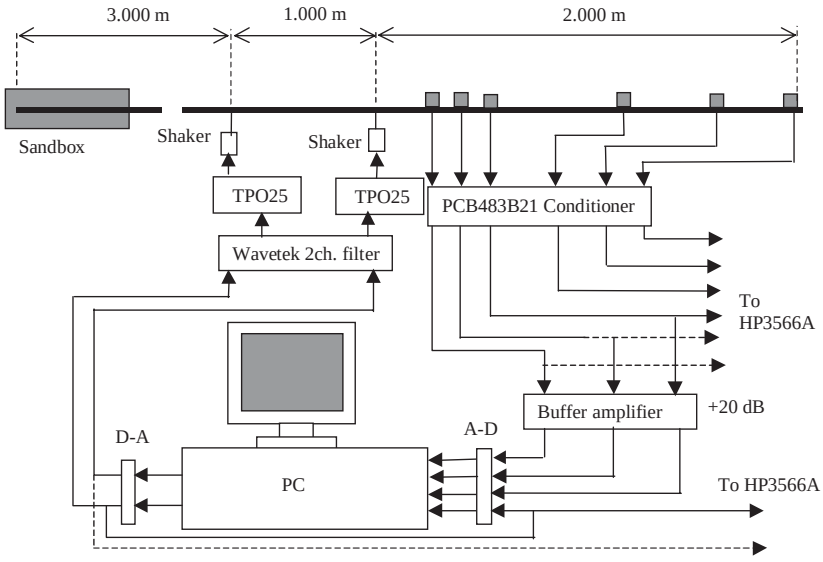

Fig. 7. Experimental set-up.

nearfield. In contrast, the second used only the third sensor in the error sensor array to give a measure of the velocity at that point. In each case, operation of the system consisted of the following steps:

1. identification of the cancellation path;
2. design of a filter to approximate the cancellation path;
3. control of vibration.

The main differences between the numerical and experimental implementations are that the sensor and actuator dynamics are fully included, that quantisation errors are present due to A–D and D–A conversion and that there is some reflection from the 'upstream' end of the beam, because the sandbox does not provide a perfectly anechoic termination.

For both the cancellation path identification and the control implementation, the disturbance signal was generated using the Simulink® random number generator. This was output directly via a D–A conversion for the cancellation path identification, while for the control implementation it was digitally bandpass filtered (200–800 Hz) prior to D–A conversion. The resulting analogue signal was then low-pass filtered (900 Hz cut-off, constant delay) to eliminate high-frequency components, amplified and used to drive the disturbance shaker. The unfiltered output was also input to one A–D channel as the reference signal.

6.3. Experimental results

In this section, the results of control using both wave-based and velocity-based control systems are presented. The results are presented in terms of the rms velocity of the beam tip before and after control.

Table 2
Parameters used in experimental measurements

Sample rate f_s	2048 Hz
Nyquist frequency f_n	1024 Hz
Wavenumber/freq relationship	$k = 0.842\sqrt{f}$
Wavelength at Nyquist frequency λ_n	0.233 m
Frequency range	200–800 Hz ($\approx 0.2f_n$–$0.8f_n$)
Wave filter length n_t	11 terms ($n_d = 5$)
Cancellation path filter length	32 terms
Control filter length	64 terms
Adaptation parameter μ	0.001
Sensor spacing Δ	0.0235 m ($\approx 0.1\,\lambda_n$)
x_s	0
x_c	1 m ($\approx 4.3\,\lambda_n$)
Centre of error sensor array x_e	1.047 m ($\approx 4.5\,\lambda_n$)
Position of point velocity error sensor x_{ev}	1.0705 m ($\approx 4.6\,\lambda_n$)
x_r	3 m ($\approx 12.9\,\lambda_n$)
x_2	3 m
Reconstruction (anti-alias) filter cut-off	900 Hz

In Fig. 8 are shown the results of wave-based control. It is apparent that there is relatively good agreement between the experimental results and the simulation, and that good attenuation is achieved throughout the specified frequency range.

The control achieved using the velocity-based control system is shown in Fig. 9. Frequency bands of poor attenuation are readily apparent, these corresponding to frequencies at which the error sensor is located close to a node of the standing wave emanating from the free end of the beam. Overall, there is qualitative agreement between the experimental results and the simulations, but the level of attenuation achieved is significantly poorer than that predicted. This is particularly evident in those frequency ranges where low attenuation was predicted. The error sensor output in these ranges is inherently low, owing to its position being close to a node. This makes the control system more sensitive to measurement and other errors, increasing the likelihood of discrepancies between simulations and experiments. It is also evident that the attenuation achieved is significantly poorer than that achieved with wave-based control. This is more easily seen in Fig. 10, which shows the attenuation achieved using the two different control strategies.

The effects of varying the control filter length are shown in Fig. 11. It is apparent that the 32, 64 and 128 term control filters give very similar performance at higher frequencies. At lower frequencies, however, the control filter length is more critical, with the 32-term filter giving significantly poorer performance. The difference between the 64 and the 128 term filters is relatively small, though, indicating that the 64 term filter is a good compromise between filter length and performance.

Fig. 12 shows the effects of varying the length of the filters used to estimate the wave amplitudes. The graph shows the response of the beam with wave filters having 11, 15 and 23 terms. It is apparent that there is no significant benefit in increasing the wave filter length beyond 11 terms in this case, and similar results were obtained with wave filters having 7 terms. In

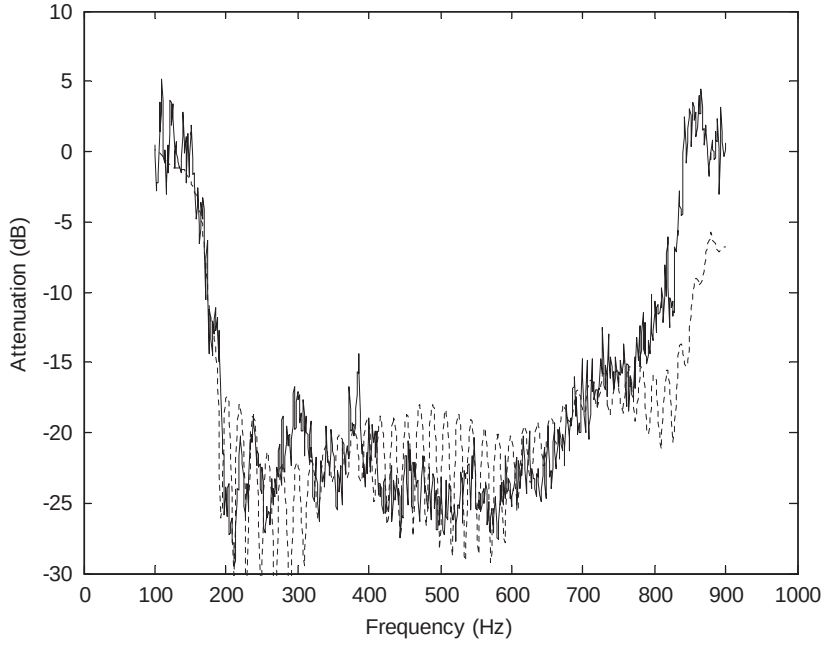

Fig. 8. Wave-based control of beam (free end): ——— experiment; ····· simulation.

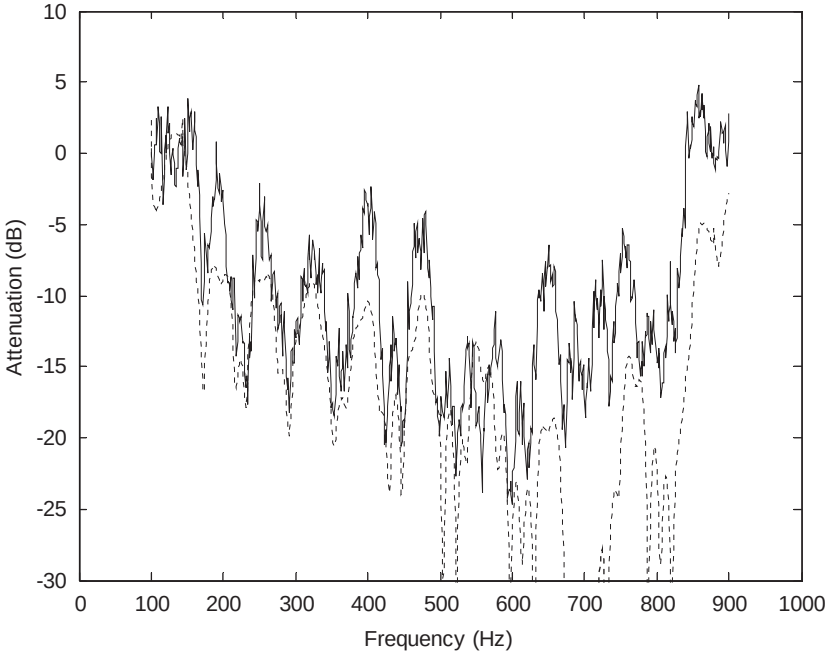

Fig. 9. Velocity-based control of beam (free end): ——— experiment; ····· simulation.

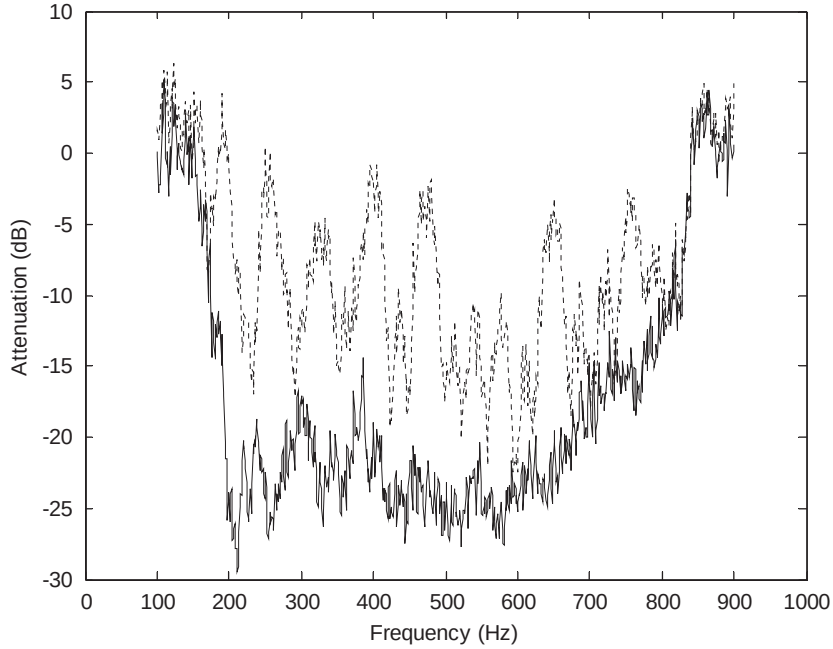

Fig. 10. Control of beam (free end): ——— wave-based control; ····· velocity-based control.

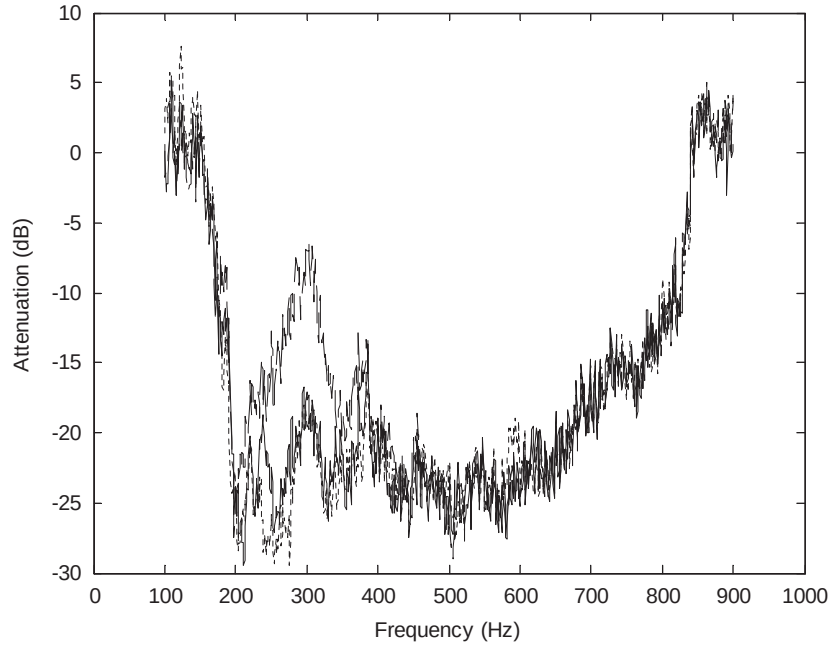

Fig. 11. Wave-based control of beam (free end): — — — 32; ——— 64 and; ····· 128 term control filters.

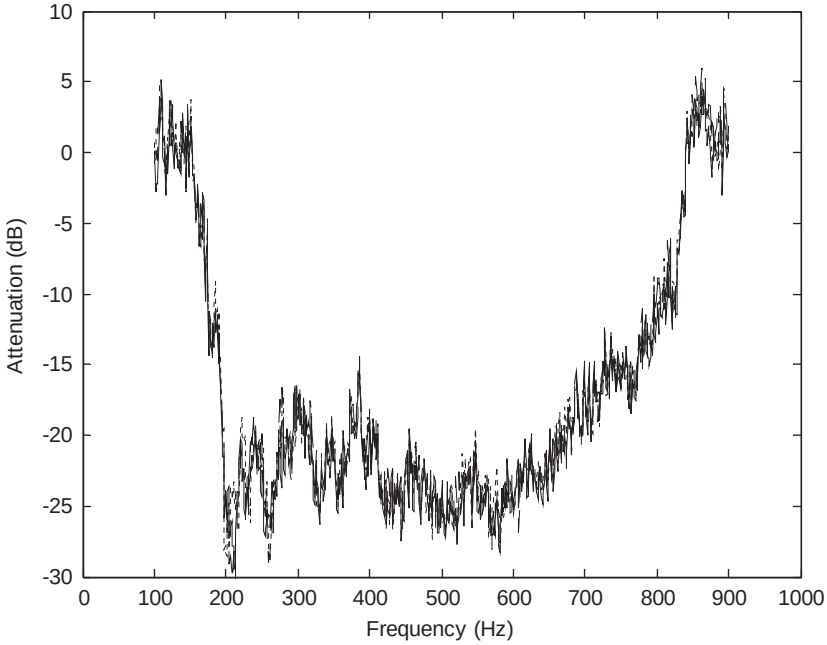

Fig. 12. Wave-based control of beam (free end): ——— 11; — — — 15 and; ····· 23 term wave filters.

practice, increasing the length of the wave filters increases the frequency range over which the required frequency responses are approximated to a reasonable degree of accuracy, but does not greatly reduce the error within that band. There is thus little to be gained by increasing the wave filter length beyond that which gives a reasonable approximation of the required frequency responses within the frequency range of interest. Furthermore, it should be noted that increasing the number of wave filter terms increases the delay in the system and may also necessitate increasing the number of terms in the cancellation path filter.

Experimentation also included variation of the cancellation path filter lengths. Filters having lengths of 16, 32 and 64 were used, and all gave very similar performance. The use of a 32-term filter for this work is therefore considered appropriate. It should be noted, however, that earlier experimental work [11] has indicated that the use of an excessively short cancellation path filter can result in slow convergence of the control system and poor overall performance.

The experiments also indicate that the adaptation parameter, μ, may be larger for the wave-based system than for the velocity-based system, thus permitting faster adaptation. This is to be expected because the maximum value of μ depends on the conditioning of the input correlation matrix, which is better in the case of wave-based control.

7. Concluding remarks

The feasibility of the proposed wave-based adaptive feedforward vibration control system, in which the propagating wave amplitude is estimated from the outputs of three sensors

located within the nearfield of the control actuator, and used as a cost function, has been demonstrated both in simulations and experimentally. The performance of this system was compared in simulations with a conventional (single sensor) velocity-based system, and with a system that uses an estimate of propagating wave amplitude obtained from the outputs of two sensors under the assumption of far-field conditions. These simulations indicate that the three-sensor system can give substantially better performance than the other systems in situations where reflections are strong and the physical space available for the control system is limited. These conditions are typical of potential applications for active vibration control. The three sensor and single sensor systems have also been compared experimentally. The results obtained are consistent with the simulations, both in terms of the characteristics shown and the levels of attenuation achieved. In summary, the three sensor wave-based system allows the use of a more physically compact control system (i.e. the error sensor can be located closer to the control actuator), and gives better overall performance than the velocity-based system under realistic conditions. The experiments also indicate that the adaptation parameter, μ, may be larger for the wave-based system than for the velocity-based system, thus permitting faster adaptation.

Acknowledgements

The authors gratefully acknowledge the financial assistance provided by the New Zealand Foundation for Research, Science and Technology, and the support of Industrial Research Ltd. in this work.

References

[1] S.J. Elliott, L. Billet, Adaptive control of flexural waves propagating in a beam, *Journal of Sound and Vibration* 163 (1993) 295–310.
[2] B.R. Mace, Active control of flexural vibrations, *Journal of Sound and Vibration* 114 (1987) 253–270.
[3] J. Scheuren, Active attenuation of bending waves in beams, *Proceedings of the Institute of Acoustics* 12 (1990) 623–629.
[4] X. Pan, C.H. Hansen, Effect of error sensor type and location on the active control of beam vibration, *Journal of Sound and Vibration* 165 (1993) 497–510.
[5] G.P. Gibbs, C.R. Fuller, R.J. Silcox, Active control of flexural and extensional power flow in beams using real time wave vector sensors, *Proceedings of the 2nd Conference on Recent Advances in Active Control of Sound and Vibration*, Blacksburgh, VA, 1993, pp. 909–925.
[6] A.E. Schwenk, S.D. Sommerfeldt, S.I. Hayek, Adaptive control of structural intensity associated with bending waves in a beam, *Journal of the Acoustical Society of America* 96 (1994) 2826–2835.
[7] A.H. von Flotow, J.B. Schafer, Wave absorbing controllers for a flexible beam, *Journal of Guidance and Control* 9 (1986) 673–680.
[8] N. Tanaka, Y. Kikushima, Optimal vibration feedback control of an Euler–Bernoulli beam: towards realization of the active sink method, *Journal of Vibrations and Acoustics* 121 (1999) 174–182.
[9] P. Audrain, P. Masson, A. Berry, Investigation of active structural intensity control in finite beams: theory and experiment, *Journal of the Acoustical Society of America* 108 (2) (2000) 612–623.
[10] B.R. Mace, C.R. Halkyard, Time domain estimation of response and intensity in beams using wave decomposition and reconstruction, *Journal of Sound and Vibration* 230 (2000) 561–589.

[11] C.R. Halkyard, B.R. Mace, Feedforward adaptive control of flexural vibration in a beam using wave amplitudes, *Journal of Sound and Vibration* 254 (1) (2002) 117–141.
[12] B.S. Widrow, S.D. Stearns, *Adaptive Signal Processing*, Prentice-Hall, Englewood Cliffs, NJ, 1985.
[13] B.R. Mace, C.R. Halkyard, Real-time measurement of wave amplitudes and intensity in a beam in the presence of a nearfield, Institute of Sound and Vibration Research Technical Memorandum TM 909, 2004.
[14] X. Pan, C.H. Hansen, Effect of end conditions on the active control of beam vibration, *Journal of Sound and Vibration* 168 (1993) 429–448.